Limitations imposed by birefringence uniformity on narrow-linewidth filters based on mode coupling

Franck Chollet*
Jean-Pierre Goedgebuer
Gadang Ramantoko
Université de Franche-Comté
Laboratoire d'Optique P.-M. Duffieux
UMR CNRS 6603
Institut des Microtechniques
F-25030 Besançon Cedex
France

Abstract. Integrated tunable narrow-linewidth wavelength filters based on TE-TM mode conversion require a high quality processing. The discussion is based on numerical simulations of typical technology-induced defects and on a comparison with experimental results. We show that uniformity of the $LiNbO_3$ crystal growth currently limits the linewidth to about 0.6 nm for spectral filters operating at 1.55 μm. Moreover, such a filter would require a technology with strict conditions of uniformity over several centimeters. The discussion is focused on electro-optic filters but the results can be extended to any device based on codirectional mode coupling, such as acousto-optic filters. [DOI: 10.1117/1.1418711]

Subject terms: integrated optics; tunable filters; birefringence; apodization; modes coupling; optical fabrication.

Paper 010038 received Feb. 8, 2001; revised manuscript received June 26, 2001; accepted for publication June 28, 2001.

1 Introduction

Wavelength division multiplexing (WDM) or optical frequency density multiplexing (OFDM) require key devices such as multiple wavelength laser sources, frequency converters, and tunable narrow-linewidth spectral filters.[1] Though DBR and DFB laser diodes have already attained very good performance in terms of power, wavelength agility, and narrow linewidth,[2] manufacturing integrated tunable narrow optical filters poses a number of technological problems that still remain to be solved. Much work has been devoted during the last 15 years to develop tunable narrow filters based on various physical principles: cascade of Mach-Zehnder interference filters,[3] asymmetrical directional couplers,[4] Bragg reflector grating filters,[5] acousto-optic filters,[6] and electro-optic filters.[7] We deal more specifically with the limitations imposed by the technological process on the linewidth of the last two types of filters based on TE-TM mode conversion. Two main parameters, the coupling coefficient and the phase birefringence, govern the filtering properties of such filters. Much work has been devoted to the influence of the coupling coefficient on the filter transmittance,[8] but the influence of phase-birefringence defects seems to be underestimated in most of the results reported so far. The latter are so small (typically a few 10^{-5}) from a region of a waveguide to the next that they can hardly be directly measured. However, in the specific case of spectral TE-TM converters/filters with a narrow linewidth, i.e., based on long interactions of light within the waveguide, their resulting cumulative action is responsible for large distortions in the spectral transmission curve.

In Sec. 2 we briefly recall the principle of a TE-TM converter filter and the digital model used to describe its behavior when it is affected by three typical types of birefringence deviation. This allows us, in Sec. 3, to investigate the filtering limitations for mode coupling-based filters working around 1.55 μm. In the next section, we validate our model by comparison with experimental and literature results, and we try to characterize the cause of the deviation. This allows us to develop in Sec. 5 the hypothesis that the technological process is liable for the birefringence deviations within the waveguide that affect the working conditions of the filter. We discuss at the same time the ultimate limitations of such a filter.

2 Modeling the Filtering Properties

We focus the discussion on integrated electro-optic filters, such as those reported by Alferness in Ref. 7. A complete description of the device can be found in Ref. 9 and we briefly recall its principle of operation. The device in its basic configuration consists of a tunable, wavelength selective electro-optic polarization converter set between two crossed polarizers (Fig. 1). The tunable polarization converter is formed by TE-TM mode coupler (or conversion) sections interleaved with phase shifter (or tuning) sections.

The conversion between the fundamental TE and TM modes with propagation constants β_{TE} and β_{TM}, is induced by a periodic index perturbation with a period Λ verifying:

$$\beta_{TM}(\lambda_0)-\beta_{TE}(\lambda_0)=\frac{2\pi}{\Lambda}$$

$$\Leftrightarrow \lambda_0=\Delta n_{ph}(\lambda_0)\Lambda, \quad (1)$$

*Current affiliation: Nanyang Technological Univ., School of MPE, 50, Nanyang Ave., Singapore 639798; E-mail: mfachollet@ntu.edu.sg

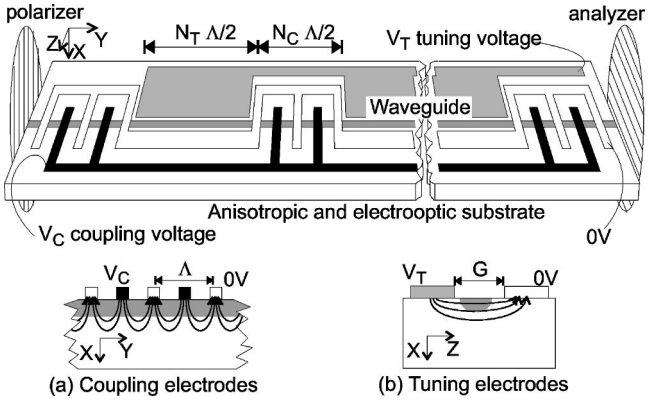

Fig. 1 Integrated polarization converter/wavelength filter. Insets (a) and (b) show the electrical fields along the X and Z axis induced by the interdigital and planar electrodes, respectively.

where λ_0 is the central wavelength of the filter and $\Delta n_{\mathrm{ph}}(\lambda_0)$ the phase birefringence. The periodic index perturbation is created via the electro-optic coefficient r_{42} and an alternative X field induced by interdigital electrodes [inset (a) in Fig. 1]. The dispersion of Eq. (1) and the two polarizers convert this polarization conversion into a wavelength filtering. The full width at half maximum (FWHM) of the filter is ideally given by[9]:

$$\delta\lambda \simeq 0.8 \frac{\lambda_0^2}{\Delta n_{\mathrm{gr}}(\lambda_0) L}, \tag{2}$$

where $\Delta n_{\mathrm{gr}}(\lambda_0)$ is the waveguide group birefringence at λ_0, and L is the filter length.

Tuning the wavelength λ_0 is obtained by changing the waveguide modal birefringence β_{TM} to β_{TE} through the electro-optic coefficients r_{13} and r_{33} with a set of tuning electrodes, which induces a Z field in the waveguide [inset (b) in Fig. 1].

Owing to the very low index difference in the waveguide, the two modes are almost pure TE and TM modes, and thus are mainly polarized along, respectively, the Z and X axis. Thus, we may use the Jones calculus[10] to model the behavior of the device, where the two orthogonal states of polarization are simply the two fundamental modes of the waveguide. However, instead of modeling each tuning and coupling section as a single (2,2) polarization transformation matrix, as reported by Heismann and Alferness,[9] we have divided[11,12] the device in N elementary cells of length $\Lambda/2$, where the matrix elements are assumed to be constant. This later simplification will appear to be not too restrictive and yields results in good agreement with the analytic formula. This numerical treatment, already used for acousto-optic filters,[13] allows us to evaluate the transmittance when some physical parameters change along the waveguide. Thus, the transformation matrix $\mathbf{T}$ for the complete filter is given by

$$\begin{aligned}\mathbf{T} = \mathbf{A}\mathbf{T}_N \mathbf{T}_{N_S(N_C+N_T)-1} \cdots \\ \cdots \mathbf{C}_{N_C+N_T+1} \mathbf{T}_{N_C+N_T} \cdots \\ \cdots \mathbf{T}_{N_C+2} \mathbf{T}_{N_C+1} \mathbf{C}_{N_C} \cdots \mathbf{C}_2 \mathbf{C}_1 \mathbf{P},\end{aligned} \tag{3}$$

where $\mathbf{P}$, $\mathbf{A}$, $\mathbf{C}_i$, $\mathbf{T}_i$, stand for the polarization transformation matrices of the polarizer, the analyzer, the i'th elementary cell inside a conversion section and the i'th elementary cell inside a tuning section, respectively. N_S is the number of coupling and tuning sections in the whole filter, and N_C and N_T are the numbers of elementary cells inside the coupling and the tuning sections, respectively.

The matrix $\mathbf{T}_i$ of the i'th elementary cell in a tuning section is derived by considering the first order perturbation induced on the propagation constant by the electric fields,[14] and is expressed as:

$$\begin{aligned}\mathbf{T}_i = &\begin{pmatrix} \exp(+j\Sigma_i \Lambda/2) & 0 \\ 0 & \exp(-j\Sigma_i \Lambda/2) \end{pmatrix} \\ &\times \exp(-j\Phi_i + \Delta\Phi),\end{aligned} \tag{4}$$

where $\Sigma_i = \Delta n_{\mathrm{ph}}^i \pi/\lambda + \Delta\beta_{\mathrm{TM}} - \Delta\beta_{\mathrm{TE}}$, $\Delta\beta_{\mathrm{TM}} \approx \pi V_T/\lambda_0 G\, n_X^3 r_{13} \Gamma_{\mathrm{TM}}$, $\Delta\beta_{\mathrm{TE}} \approx \pi V_T/\lambda_0 G\, n_Z^3 r_{33} \Gamma_{\mathrm{TE}}$, n_X and n_Z are the principal indices of lithium niobate along the X and Z axes, Γ_{TE} and Γ_{TM} are the overlap coefficients between the applied electrical field and the optical field of the TE and TM modes, respectively, and $\Phi_i = (\beta_{\mathrm{TM}}^i + \beta_{\mathrm{TE}}^i)\Lambda/4$, $\Delta\Phi = (\Delta\beta_{\mathrm{TM}} + \Delta\beta_{\mathrm{TE}})\Lambda/4$.

The matrix $\mathbf{C}_i$ in Eq. (3) is the polarization conversion matrix of the i'th elementary cell in a coupling section, which is derived using piece-wise integration of the equations appearing in the coupled mode formalism[15,12]:

$$\begin{aligned}\mathbf{C}_i = &\begin{pmatrix} a_i \exp(+j\delta_i \Lambda/2) & b_i \exp(+j\delta_i \Lambda/2) \\ -b_i^* \exp(-j\delta_i \Lambda/2) & a_i^* \exp(-j\delta_i \Lambda/2) \end{pmatrix} \\ &\times \exp(-j\Phi_i),\end{aligned} \tag{5}$$

where $a_i = \cos(\Delta_i \Lambda/2) + j\,\delta_i/\Delta_i \sin(\Delta_i \Lambda/2)$ and $b_i = -j\,\kappa/\Delta_i \sin(\Delta_i \Lambda/2)$ with

$$\Delta_i = \sqrt{\kappa^2 + \delta_i^2},$$

$$\kappa = \frac{\pi}{\lambda_0} \sqrt{n_X^3 n_Z^3} r_{41} \frac{V_C}{\Lambda/4} C^1_{\Gamma_{\mathrm{TE-TM}}}$$

is the coupling coefficient, and $\delta_i = \Delta n_{\mathrm{ph}}^i(\lambda)\pi/\lambda - \pi/\Lambda$ is the relative phase mismatch. We have improved on the classical solution[9] by using the first Fourier coefficient in the development of the overlap function between the optical and electrical fields, $C^1_{\Gamma_{\mathrm{TE-TM}}}$, instead of $\Gamma_{\mathrm{TE-TM}}$ itself.[12] The coupling coefficient κ is the same in all the cells because, as we see in Sec. 5, it seems that the process imperfections do not affect it substantially.

For TE mode input and TM output, the input polarizer and output analyzer are respectively described by the matrices $\mathbf{P}$ and $\mathbf{A}$ given by:

$$\mathbf{P}=\begin{pmatrix}1 & 0\\ 0 & 0\end{pmatrix} \quad \text{and} \quad \mathbf{A}=\begin{pmatrix}0 & 0\\ 0 & 1\end{pmatrix}. \tag{6}$$

To investigate the effects of the birefringence deviation on the transmittance profile, we take a birefringence that varies along the waveguide, that is

$$\Delta n_{\mathrm{ph}}^{i}=\Delta n_{\mathrm{ph}}+\mathrm{dn(i)}, \tag{7}$$

where Δn_{ph} is the normal birefringence and dn(i) is the birefringence deviation for the i'th section. We choose three broad classes of deviation that are justified later: a random deviation, a symmetrical deviation with the symmetry center in the middle of the filter, and a monotone deviation.

$$\mathrm{dn(i)}=\begin{cases}\delta n\ \mathcal{N}(0,1) & \text{random}\\ \pm\delta n\left(\dfrac{i-N/2}{N/2}\right)^{2} & \text{parabolic}\\ \delta n\dfrac{i-N/2}{N/2} & \text{linear}\end{cases}. \tag{8}$$

We use a linear variation as the odd function needed to simulate the monotone deviation, while a parabolic variation is taken as the even function to model the symmetrical deviation. We checked that any other odd (respectively even) functions yield results similar to the linear (respectively parabolic) case. For the random case, $\mathcal{N}(0,1)$ is the standard normal distribution ($\mu=0$ and $\sigma=1$). Figure 2 shows the filter transmittance calculated for these three types of birefringence deviation.

In the case of a monotone deviation of birefringence [Fig. 2(a)], the birefringence varies continuously along the waveguide above and below the birefringence Δn_{ph} at the middle of the filter. Thus the phase-matched condition in Eq. (1) is now also verified for wavelength above and below λ_0, increasing their transmittance and gradually merging the sidelobes with the central lobe. Moreover, the filter maximum transmittance decreases. Canceling out this later effect by increasing the coupling coefficient ($\kappa=1.8\kappa_0$ restores a 100% transmittance at λ_0) is plagued by a further increase of the sidelobe transmittance and of the FWHM. The effect of a parabolic deviation has already been discussed for the acousto-optic filters.[16,13] For a negative symmetric deviation [Fig. 2(b)], the birefringence decreases at each end of the filter, with its maximum value at the middle. Thus the phase-matched condition is also verified for wavelengths lower than λ_0, increasing their transmittance. For a positive parabolic deviation, the effect is opposite, and we observe an increase of the sidelobes for high wavelengths and a decrease in the other side of the spectrum. Interestingly, the zeros of the transmission curve are not affected. The overall shift of the transmittance toward lower wavelengths is due to the change in the mean birefringence of the filter for the parabolic case in Eq. (8) ($\overline{\Delta n_{\mathrm{ph}}^{i}}=\Delta n_{\mathrm{ph}}+\delta n/3$).

When the filter features simultaneously a linear and a parabolic birefringence deviation, the transmittance features a combination of the two previous effects. Numerical simulations show that the filter characteristics can be approximated by computing the effects of the two deviations separately. Namely, its FWHM will be the FWHM of a filter of same length with the linear deviation alone, and the level of its sidelobe will be that of a filter featuring the parabolic deviation only. This holds especially for small birefringence deviations ($<5\cdot10^{-5}$), even if the set of equations describing the filter behavior altered by birefringence deviation is not linear.

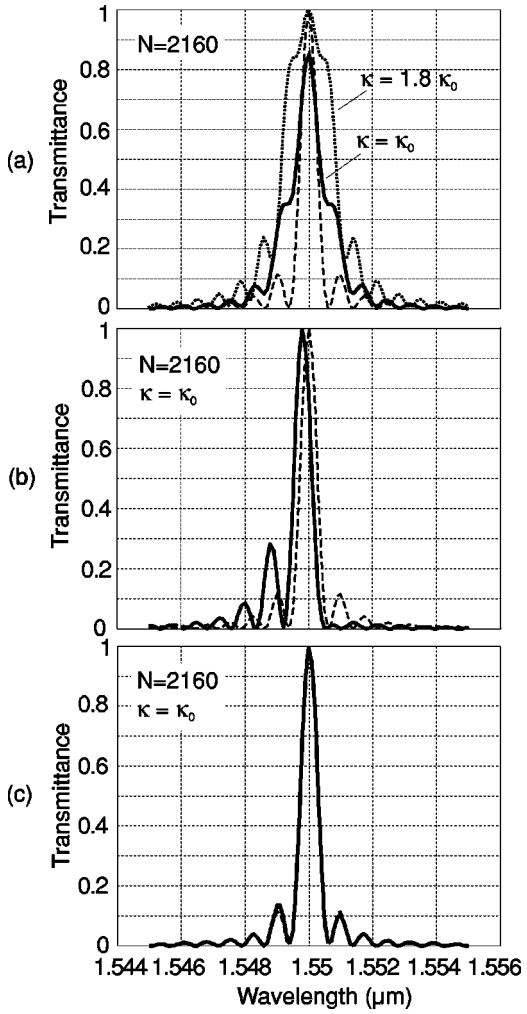

Fig. 2 Filter transmittance for (a) linear, (b) negative parabolic, and (c) typical random birefringence deviation with $\delta n=5\cdot10^{-5}$ and $N=2160$, i.e., a filter length of 46 mm. For comparison, the dashed curves show the transmittance of an ideal filter ($\lambda_0=1.55$ μm, $V_T=0$ V). The coupling coefficient κ is expressed in function of $\kappa_0=\pi/2L\ N_C/N_C+N_T$ that would yield a 100% transmittance at λ_0 for a filter with a constant birefringence.[9]

Comparatively, a random birefringence deviation has less impact on the filter transmittance, as shown in Fig. 2(c). Nevertheless, a random variation in the conversion efficiency for all the wavelengths is observed with a slight decrease of the maximum transmittance. Further investigations indicate that significant degradations of the filter transmittance start to be observed when $\delta n\geqslant35\cdot10^{-5}$.

With this model, tuning the filter to another wavelength ($V_T>0$ V) creates a negligibly small degradation in the original filter transmittance. Actually, the mean birefringence in the waveguide is changed but the change induced

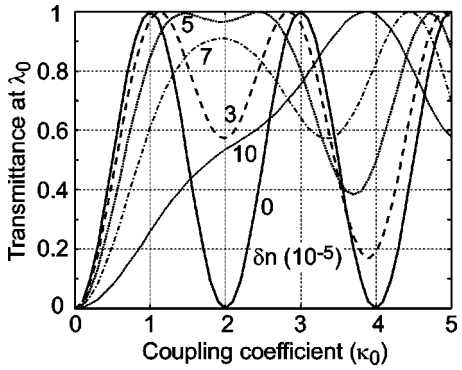

Fig. 3 Calculated evolution of the maximum of transmittance versus the normalized coupling coefficient for different values of a linear birefringence deviation ($N=2160$, $\lambda_0=1.55$ μm).

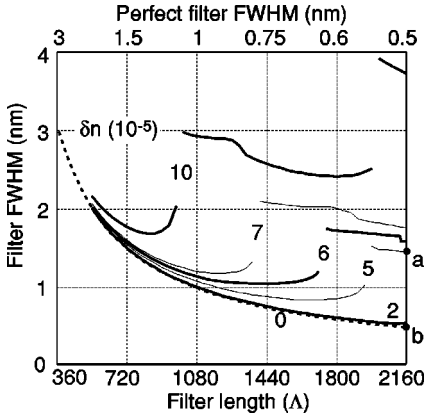

Fig. 4 Digital simulation of the FWHM versus the filter length for different values of the linear birefringence deviation (δn) and for $\lambda_0=1.55$ μm. The dotted curve is obtained after Eq. (2) for a perfect filter using $\Delta n_{gr}=0.0825$ and $\Lambda=21.4$ μm. (We reported the values on the top scale for comparison.) For $N=2160$, the profile of the transmittances at points (a) and (b) are given in Fig. 2(a) for the curve with $\kappa=1.8\kappa_0$ and the dotted curve, respectively.

by the tuning voltage is almost position independent and thus it does not add any birefringence gradients.

3 Limitations Induced by the Birefringence Deviations

We now explore the limitations introduced by the birefringence deviation when fabricating a narrow bandpass filter. Matching exactly the experimental transmittance with the simulation is a complex problem when different types of deviations are combined together. Thus, we have chosen to consider some significant features of the transmittance and tried to find a correlation with the birefringence deviation. The main limitations to consider deal with the transmittance maximum, the linewidth of the filter, and the level of the sidelobes that determines the level of cross talk in applications on dense wavelength multiplexing.

3.1 *Limitations Imposed on the Transmittance Maximum*

In a first step, we analyze the evolution of the transmission peak of a narrow filter (FWHM = 0.5 nm) with the monotone birefringence deviation. Figure 3 shows that the sine exchange of energy, which is known to occur for a perfect filter[15] with $\delta n=0$, evolves quickly as the birefringence deviation increases. With a 10^{-4} birefringence deviation, to obtain a high conversion efficiency (20 dB or 99%), we need a coupling coefficient 3.8 times larger than that of the ideal device. Practically, this means an operating voltage 3.8 times larger than for the perfect filter.

The influence on the transmittance maximum of a random and a symmetric deviation of birefringence is very small and can be neglected in a first approximation.

3.2 *Limitations Imposed on the Filter Linewidth*

In a second step, we computed the FWHM of filters versus their lengths for different monotone birefringence deviations (Fig. 4). As δn increases, the maximum transmittance of the filter is reduced, except if the coupling coefficient (i.e., the conversion voltage) is increased. Thus we used for the computation an optimal coupling coefficient defined as the lowest one yielding a maximum transmittance of 99%. For example, in the case depicted in Fig. 2(a), the optimal coupling coefficient will be $1.8\kappa_0$. The effective FWHM of the filter is then defined as the central lobe linewidth at 50% obtained with this optimal coupling coefficient.

To validate further the numerical model expressed by Eqs. (3)–(6), we have also drawn in Fig. 4 the analytical curve given by Eq. (2) in the case of a perfect filter. The curve thus obtained is exactly superimposed with the curve $\delta n=0$ of the numerical model. For $\delta n>0$, as the device length is increased, Fig. 4 shows that the filter FWHM decreases down to a minimum and starts to increase. In that last part of the curve, the *longer* the device is, the *wider* the filter FWHM is! This point has been completely overlooked in previous works and does not appear when using the analytical expression of Eq. (2). This effect starts earlier for large birefringence deviations as can be clearly seen in Fig. 4. This behavior can be understood by considering the interference occurring at the device output. At the central wavelength, all the partially converted waves (or wavelets) interfere constructively at the output to yield a 100% transmittance. But, this ideal situation is corrupted by the birefringence deviation that disturbs the phase of the wavelets. Thus, a reduced number of wavelets can interfere constructively at the device output. It can be overcome by increasing the local coupling coefficient, as explained before. For long devices (i.e., narrow FWHM), a very small local phase error spoils the transmittance since a very high number of wavelets is expected to interfere constructively at the device output. The jumps observed in the curves are necessary to keep the maximum transmittance above 99%. After a region where the coupling coefficient needs to be increased continuously, we have to jump to the next maximum in the transmittance. For example, in the case of Fig. 2(a), we can see in Fig. 3 that we need to have $\kappa=1.8\kappa_0$, because the peak at about $\kappa\approx\kappa_0$ has too low of a transmittance. Still, note that the jump appears substantially *after* the minimum of the FWHM curve is attained and thus does *not* affect the existence and position of the minimum.

Figure 4 also gives an estimate of the quality of the technological process needed to achieve a filter with a given linewidth. It is worth noting that to obtain a 0.5-nm-

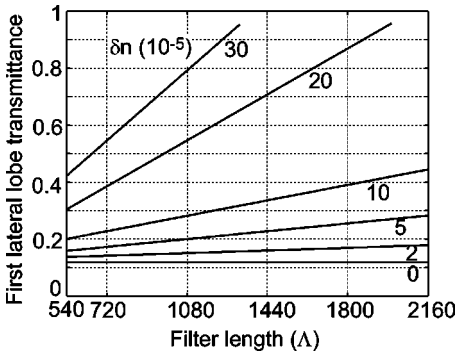

Fig. 5 Numerical simulation of the evolution of the first sidelobe transmittance with the device length for different parabolic birefringence deviation ($\lambda_0 = 1.55\ \mu$m).

linewidth filter instead of a 1-nm-linewidth filter, it is not enough to increase the device length by a factor of 2. We also need to improve the technology to decrease the magnitude of the eventual birefringence deviation by a factor of 3. Moreover, the filter length and the FWHM are not simply governed by Eq. (2); the length has to be increased substantially in comparison with a perfect filter to obtain the desired linewidth.

Again, we have also studied the limitation imposed on the filter FWHM by the magnitude of the symmetric deviation of birefringence. This effect may again be neglected in view of the large sensitivity of the lateral lobe level to such deviation, as we see now.

3.3 *Limitations Imposed on the Level of the Sidelobes*

Even though a symmetric deviation of birefringence has few effects on the transmittance of the main lobe and on the FWHM, it may still degrade the filter transmittance by increasing quickly the sidelobe level. In Fig. 5, the sidelobe level is plotted as a function of the filter length for different values of the parabolic birefringence deviation. For large values of δn ($>10^{-4}$), we observe a slight decrease of the maximum transmittance if we keep the coupling coefficient $\kappa = \kappa_0$. Therefore the curves are plotted using the optimal coupling coefficient as defined previously.

The relationship between the lateral lobe level and the length of the filter with a given parabolic birefringence deviation appears to be linear. If we want to keep the sidelobe level below 20% rather than 12% as expected theoretically for an ideal filter, we see that the birefringence deviation has to be very small to satisfy the requirements of a narrow-linewidth filter, for example below $3 \cdot 10^{-5}$ for a 0.5-nm FWHM filter. The $\delta n = 10^{-4}$ parabolic birefringence deviation discussed previously would increase the sidelobe level to 50%, making indeed the device useless in most applications.

Linear deviation of birefringence also modifies the level of the sidelobes. However, this effect is much smaller than the equivalent parabolic deviation, and thus may usually be neglected.

Finally, we may note that the effects of the parabolic deviation starts with a smaller deviation magnitude than the FWHM broadening seen before. Actually, even short filters will be significantly affected by such deviation and it is likely that the increase in the sidelobe transmission will be observed more often than the broader central lobe, which will mainly affect long filters (i.e., filters with a FWHM <1 nm).

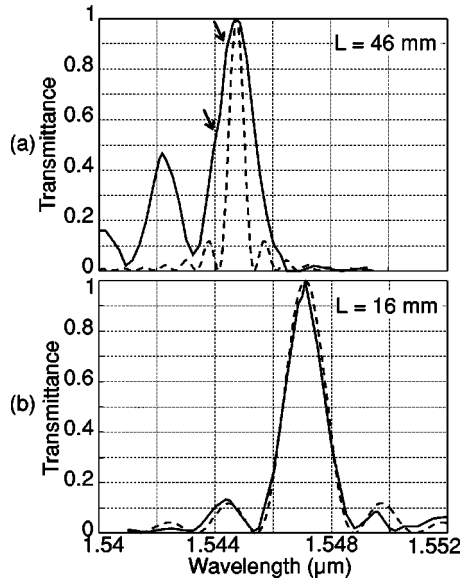

Fig. 6 Experimental spectral transmission curve of (a) a 46-mm and (b) a 15-mm-long filter obtained using the same process. Dashed curves show the theoretical transmittance obtained with Eq. (3) for $\delta n = 0$, and $\lambda_0 = 1.55\ \mu$m, $\kappa = \kappa_0 = \pi/2L$, using (a) $N = 2160$ and (b) $N = 720$ elementary cells.

4 Observation of Filter Limitations

We now use our model to comment on experimental results obtained in our laboratory and in the literature.

Figure 6 shows the theoretical and experimental spectral transmittance curves for two devices with different lengths (15 and 46 mm). The experimental results were obtained for two devices fabricated in our laboratory with the same standard process.[12]

We observe that the discrepancy between the experimental and theoretical curves is very large in the case of the long filter. In addition to a broader central lobe and strong asymmetrical sidelobes, the mode-coupling voltage V_C required to get the maximum transmittance is increased by a factor of 3.2 when compared with the model (10 V, with $C^1_{\Gamma_{\mathrm{TE-TM}}} = 0.08$,[12] to be compared with an experimental value of 32 V). On the other hand, the short filter behaves essentially as predicted by a model where the birefringence deviation is neglected. These first results indeed show that the cause of these effects creates larger transmittance distortions for long filters than for short ones.

However, a direct measurement of the birefringence deviation is difficult to obtain (with an acousto-optic filter, the pulse-probing technique may indirectly determine such a variation[17]). Still we obtained an indirect proof of a monotonic birefringence gradient with the long filter by cutting it in two parts of the same length.[12] The two half filters featured two different center wavelengths $(\lambda_0)_1$ and $(\lambda_0)_2$, spaced by 1.1 nm. This can be attributed to a mean birefringence difference of $5.5 \cdot 10^{-5}$ along the filter, corre-

sponding to $\delta n \approx 5.5 \cdot 10^{-5}$ in the model. In Fig. 4, the curve obtained for $\delta n = 6 \cdot 10^{-5}$ best fits the characteristics of the two previous 15- and 46-mm-long filters. Actually, the longest ($N = 2160$) presents a FWHM of about 1.55 nm, slightly larger than the shortest ($N = 720$). Measurement errors (temperature drift) and also the coupled effects of the parabolic deviation could explain this slight discrepancy. Moreover, Fig. 2 shows that for such a birefringence deviation, the coupling coefficient of the long filter should be 3.8 times higher than its ideal value to obtain a good conversion efficiency. This is in good accordance with the experimental filter that needed an operating voltage 3.2 times higher than the expected value. The discrepancy between these two values may be attributed to a slight underestimation of the coefficient $\mathbf{C}^1_{\Gamma_{TE-TM}}$.

It may be observed that the small kinks, shown by an arrow on the left part of the central lobe in Fig. 6(a) and with a period of about 0.5 nm, appear to be the remnant of the lateral lobe whose transmittance has increased due to the monotone birefringence gradient, as was simulated in Fig. 2(a).

The presence of exaggerated sidelobes in the transmittance of the polarization converter-based filters has been observed since the first publications related to the subject, with either electro-optic[7,18] or acousto-optic[16,19] filters. Clearly, the maturity of the process had a beneficial effect on the magnitude of this effect. According to Fig. 5, the increase to 45% of the transmittance of the first lateral lobe in Fig. 6(a) may be attributed to a parabolic gradient of magnitude 10^{-4}. This effect should increase the transmittance of the first lateral lobe of the short filter to about 23%. However, we can see in Fig. 6(b) that its level is only about 15%, corresponding to a parabolic birefringence deviation of about $3 \cdot 10^{-5}$. Thus the magnitude of the deviation in the shorter filter is about three times smaller that in the longer one. This figure matches quite well with the ratio of the length of the two filters. This result suggests that the symmetric deviation of birefringence is proportional to the length of the filter.

It is confirmed experimentally that tuning the filter ($V_T > 0$ V) imposes a negligibly small degradation in the original filter transmittance, justifying the assumption made to develop our model.

Referring to Figs. 4 and 5, it appears that the process used for the devices presented in Fig. 6 is suited for fabricating $LiNbO_3$ filters not longer than 1400 Λ, i.e., 30 mm for a 1.55-μm operating wavelength. According to Fig. 4, the narrowest achievable linewidth that could be expected is about 1.1 nm (instead of 0.8 nm for a perfect filter of same length) without substantial process improvements. Incidentally, this value is similar to the lowest value often reported by different teams in the literature for a single pass filter.[7,13,16,18]

5 Origin of the Birefringence Deviations

We now have enough experimental evidence to justify the profile of the birefringence deviation chosen in the analysis. It is obvious that a random variation of the birefringence along the waveguide exists. However, it is less clear why systematic symmetrical and antisymmetrical birefringence deviations with a magnitude depending on the length of the filter also appear. Clearly, their origin may be split in two classes, either the gradient is induced during the operation of the filter or during its fabrication.

The large dependence of the lithium niobate refractive index with temperature ($4 \cdot 10^{-5}$ K^{-1} at 1550 nm as deduced from Ref. 20) may be at the origin of an operation-induced gradient. A difference of temperature of 2.5 K along the waveguide while the filter is operated causes a birefringence deviation of 10^{-4}. Thus, thermal grease and an aluminum plate should be placed on the back of the crystal to minimize any systematic temperature gradient. For the electro-optical filter, such approach is facilitated by the absence of heat source in the device, but with acousto-optical devices it may become more complex.[16] In any case, the heating induced by the absorption of the light inside the waveguide, that may give rise to a monotonously decreasing gradient of temperature, may be neglected: rough calculation shows that the increase in temperature is only 0.05 K with the cooling plate.

Thus it seems that the origin of the systematic gradients have to be sought in the fabrication itself. The process used for titanium in-diffused $LiNbO_3$ integrated devices is well known.[21] The waveguide is fabricated by diffusing at a high temperature a thin stripe of titanium. Generally, this step is followed by the deposition of a dielectric buffer layer, before the deposition and the patterning of the electrodes.

To estimate the impact of the process parameters on the waveguide birefringence, we have used the effective index method, with the index model described by Fouchet et al.,[22] extended to the 2-D case with the use of the standard Fick's equation and of the classical long time diffusion approximation.[12] For our standard process at $\lambda_0 = 1.55$ μm, the titanium width is 8 μm, the titanium thickness is 800 Å, the diffusion time is 8 h, and the diffusion temperature is 1016°C. We used a diffusion constant along the X axis of $4.3 \cdot 10^{11}$ μm^2/h and an activation energy along the X axis of 3.0 eV as determined separately.[12] These constants are slightly larger than those usually reported in the literature for a Y-cut crystal, however, X-cut crystals have received very little attention and no other results are known in the open literature. With these values, a birefringence deviation of about 10^{-4} may be attributed to a variation of the titanium stripe width by 0.3 μm or thickness by 10 Å, or to a diffusion temperature gradient of 2 K.[12,13]

The symmetrical deviation of birefringence may be attributed to the sputtering process used to deposit the titanium layer that has been shown to produce symmetrical deviation in the thickness on a large plate. Moreover, the width of the titanium stripe is usually considered to vary randomly with the crystal abscissa, but we have shown recently[23] that the spinning process induces a slight symmetrical variation of the stripe width from the substrate center to each of the substrate ends. For the process used to manufacture the filters in Fig. 6(a), we measured symmetrical change in the waveguide width in the order of 0.4 μm. This value would account for a deviation of $12 \cdot 10^{-5}$, close to the $11 \cdot 10^{-5}$ needed, according to Fig. 5, to explain the observed increase of the sidelobe level to 45%.

The monotone variation may also be created during the deposition of titanium when an e-beam evaporator is used. We have observed parallel interference fringes when a di-

electric material is evaporated on large size glass plates, suggesting that improper evaporation conditions result in a monotone increase of the titanium thickness with the device abscissa. Measurement of thickness variation in the order of a few Å, needed to keep the deviation to a few 10^{-5}, were not possible and we could only take corrective measures blindly (e.g., two step deposition with sample reversal). Similarly, the monotone thickness variation of the SiO_2 buffer layer evaporated over the waveguide also modifies the birefringence within the waveguide, because the optical field does not completely vanish at the niobate-SiO_2 interface. During patterning of the titanium stripe, a poor contact between the sample and the mask, usually resulting in an air wedge (that will be evidenced by the presence of fringes of equal thickness), will cause a minute change in the waveguide width that will affect the birefringence. Careful operation of the mask aligner suppresses this problem. On the other hand, during the diffusion, due to the constant gas flow often used at this step of the process for different reasons, a monotone temperature gradient along the waveguide may appear if the long crystal is placed parallel to the gas flow. Checking the temperature uniformity inside the furnace should correct this behavior, and a shielded boat (e.g., a platinum box as used in some groups) could be beneficiary.

A random birefringence deviation with $\sigma \geqslant 35 \cdot 10^{-5}$, that could significantly affect the transmittance (Sec. 2), implies that 5% of the cells should present a deviation larger than $7 \cdot 10^{-4}$ (2σ rule). This means a variation of 2 μm in the waveguide width, or of 15 K in the diffusion temperature, which is rather unlikely. Hence it seems that random deviations (due to an inhomogeneous temperature bath or UV illumination, for example) will only account for small deviation in the transmittance, and large transmittance distortion can safely be attributed to the systematic deviations.

It should be noted that the variation of the period of the conversion electrodes may also introduce an equivalent birefringence deviation by changing the phase-matched condition in Eq. 1, which will probably be random.

As we suggested in the previous section, most of the cause of birefringence deviation described here obviously depends on the length of the substrate. Thus not only does the deviation of birefringence have less effect on the short filters (Sec. 3), but the magnitude of the deviation will even be smaller, decreasing further the distortion in their transmittance. Then, the fabrication of the long filter with narrow FWHM becomes a real challenge. But this thorough study has allowed us to identify the main cause of birefringence deviation, and we were able to improve our process[12,23] to obtain a filter with 0.7-nm FWHM.[24] That is, as far as we know, the best results reported so far for a single pass polarization-conversion filter on lithium niobate.

The ultimate limitation on linewidth is dictated by a cause of birefringence deviation that we have not discussed so far: the uniformity in the $LiNbO_3$-crystal itself. Recent measurement by the NIST[25] using the Maker fringe analysis[26,27] reveals for an X-cut crystal a peak-to-peak fluctuation of the extraordinary index of $7 \cdot 10^{-5}$ (Fig. 6 in Ref. 25). This fluctuation is linked with variations in the LiO_2 molarity that do not significantly affect the ordinary index, and thus they can be taken as fluctuations of the crystal birefringence. Interestingly, as noted by the authors, these fluctuations appear to present a gradient parallel to the Y axis of about $3.5 \cdot 10^{-5}$ superimposed with random fluctuations. If our model is applied to this data, a FWHM of 0.6 nm is the best result that can be obtained for *any length* of single-pass filter on $LiNbO_3$ (the crystal needs to be about 46 mm long). We have almost attained this limit, but new improvements, such as laser writing of the conversion electrodes[28] and e-beam patterning of waveguides, may be needed to reduce further the linewidth of TE-TM spectral filters.

6 Conclusion

We show that the influence of small systematic phase-birefringence defects within a waveguide can be very important on the filter transmittance. Their cumulative effects yield large distortions on the sidelobes and on the center transmission peak. We simulate three types of defects that were assumed to be met in a conventional manufacturing process. They yield spectral transmission curves that are in very good agreement with those observed experimentally, and confirm the validity of the model and of the assumptions. Having identified the cause of the linewidth limitation, we were able to improve our manufacturing process obtaining a filter of length 44 mm with 0.7 nm FWHM, near the limit of 0.6 nm estimated from the current crystal birefringence uniformity measured by the NIST.

Besides improving crystal growth and the fabrication process, we may use alternate structures compensating for the manufacturing defects. For example, mirror-folded structures[29] have the great advantage of reducing the crystal length by a factor 2 (or more if multiple total reflections are used), and of decreasing the problems related to the birefringence deviation. This structure has been reported to yield a FWHM of 0.6 nm. Another solution is to provide along the waveguide an additional short tuning section controlled with independent voltage to compensate for the phase mismatch. However, these two solutions are plagued by a higher operation complexity to obtain phase-matched conversion along the filter, because they sharply increase the number of independent voltages to adjust. Interestingly, cascaded filters have also shown good characteristics for FWHM down to 1 nm.[30] However, decreasing the FWHM further is hindered by the availability of large crystals.

Generalizing the present results to acousto-optic TE-TM filters is straightforward using our model with $N_C = N$ and $N_T = 0$ (no tuning section).

Finally, it appears that the fabrication of a narrow TE-TM converter/filter is a very powerful tool to test the quality of fabrication processes. As we show, the analysis of the transmittance curve will help identify the problems in the fabrication steps. Moreover, their extent will be hinted at by using the curve of Figs. 4 and 5 that will decide the appropriateness of corrective measures.

References

1. K. Nosu, H. Toba, K. Inoue, and K. Oda, ''100 channel optical FDM technology and its applications to optical FDM channel-based networks,'' *J. Lightwave Technol.* **11**, 764–771 1993.
2. M. Okai, T. Tsuchiya, K. Uomi, W. Chinone, and T. Harade, ''Corrugation-pitch-modulated MQW-DFB laser with narrow spectral

linewidth (170 KHz),'' *IEEE Photonics Technol. Lett.* **2**, 529–531 (1990).
3. N. Takato, A. Sugita, K. Onose, H. Okazaki, M. Okuno, M. Kawachi, and K. Oda, ''128-channel polarization-insensitive frequency-selection switch using high-silica waveguide on Si,'' *IEEE Photonics Technol. Lett.* **2**, 441–443 (1990).
4. R. Alferness and J. Veselka, ''Simultaneous modulation and wavelength multiplexing with a tunable Ti:$LiNbO_3$ directional coupler,'' *Electron. Lett.* **21**, 466–468 (1985).
5. J. Söchtig, ''Ti:$LiNbO_3$ stripe waveguide Bragg reflector gratings,'' *Electron. Lett.* **24**, 845–847 (1988).
6. Y. Ohmachi and J. Noda, ''$LiNbO_3$TE-TM mode converter using collinear acoustooptic interaction,'' *IEEE J. Quantum Electron.* **13**, 43–50 (1977).
7. R. Alferness, ''Efficient waveguide electrooptic TE<->TM mode converter/wavelength filter,'' *Appl. Phys. Lett.* **36**, 513–515 (1980).
8. P. Cross and H. Kogelnik, ''Sidelobe suppression in corrugated-waveguide filters,'' *Opt. Lett.* **1**, 43–46 (1977).
9. F. Heismann and R. Alferness, ''Wavelength-tunable electrooptic polarization conversion in birefringent waveguides,'' *IEEE J. Quantum Electron.* **24**, 83–93 (1988).
10. R. Jones, ''A new calculus for the treatment of optical systems: I. description and discussion of the calculus,'' *J. Opt. Soc. Am.* **31**, 488–493 (1941).
11. G. Ramantoko, ''Étude et réalisation d'un filtre accordable intégré sur niobate de lithium,'' PhD thesis, Université de Franche-Comté, Besançon, France (1992) (in French).
12. F. Chollet ''Réalisation d'un filtre spectral accordable étroit à 1.55 μm en optique intégrée sur niobate de lithium. Etude des limitations imposées par la technologie,'' PhD thesis, Université de Franche-Comté, Besançon, France (1995) (in French).
13. D. Smith, A. D'Alessandro, and J. Baran, ''Source of sidelobe asymmetry in integrated acousto-optic filters,'' *Appl. Phys. Lett.* **62**, 814–816 (1993).
14. A. Yariv, *Quantum Electronics*, 3rd ed., Chap. 11, J. Wiley & Sons, New York (1989).
15. A. Yariv and P. Yeh, *Optical Waves in Crystals*, Chap. 6, J. Wiley & Sons, New York (1984).
16. W. Trutna, Jr., D. Dolfi, and C. Flory, ''Anomalous sidelobes and birefringence apodization in acousto-optic tunable filters,'' *Opt. Lett.* **18**, 28–30 (1993).
17. H. Rashid, D. Smith, Z. Bao, R. Chakravarthy, M. Pathan, N. Imam, K. Kissa, and J. Kallman, ''Use of radio-frequency pulse surface acoustic wave profilometry for passband engineering of acousto-optic tunable filters,'' *Opt. Lett.* **21**, 342–344 (1996).
18. G. Ramantoko, J.-P. Goedgebuer, and H. Porte, ''Synthesis of large optical delays by mode coupling in electro-optically tunable TE-TM mode converters,'' *Opt. Lett.* **6**, 372–374 (1996).
19. D. Smith, J. Baran, K. Cheung, and J. Johnson, ''Polarization-independent acoustically tunable optical filter.,'' *Appl. Phys. Lett.* **56**, 209–211 (1990).
20. D. Smith and H. Riccius, ''Refractive index of lithium niobate,'' *Opt. Commun.* **17**, 332–334 (1976).
21. R. Schmidt and I. Kaminow, ''Metal-diffused optical waveguides in $LiNbO_3$,'' *Appl. Phys. Lett.* **25**, 458–461 (1974).
22. S. Fouchet, A. Carenco, C. Daguet, R. Guglielmi, and L. Riviere, ''Wavelength dispersion of Ti induced refractive index change in $LiNbO_3$ as a function of diffusion parameters,'' *J. Lightwave Technol.* **5**, 700–707 (1987).
23. F. Chollet and J.-P. Goedgebuer, ''Improved $LiNbO_3$ technology for reducing sidelobe asymmetry in mode converter-based wavelength filters,'' *Jpn. J. Appl. Phys., Part 2* **37**, 979–981 (1998).
24. F. Chollet, J.-P. Goedgebuer, H. Porte, and A. Hamel, ''Electrooptic narrow linewidth wavelength tuning and intensity modulation of an erbium fiber ring laser,'' *IEEE Photonics Technol. Lett.* **8**, 1009–1011 (1996).
25. N. Sanford and J. Aust, ''Uniformity studies of congruent $LiNbO_3$ by means of maker fringe analysis'' in *Handbook of Advanced Electronic and Photonic Materials*, Hari Singh Nalwa, Ed., Academic Press, New York (2000).
26. J. Aust ''Maker-fringe analysis and electric-field poling of lithium niobate,'' PhD thesis, University of Colorado, Boulder (1999).
27. N. Sanford and J. Aust, ''Nonlinear optical characterization of $LiNbO_3$. i. theoretical analysis of maker fringe patterns for x-cut wafers,'' *J. Opt. Soc. Am. B* **15**, 2885–2909 (1998).
28. M. Haruna, T. Kato, K. Yasuda, and H. Nishihara, ''Laser beam periodic-dot writing for fabrication of Ti:$LiNbO_3$ waveguide wavelength filters,'' *Appl. Opt.* **33**, 2317–2324 (1994).
29. F. Heismann, M. Divino, and L. Buhl, ''Mirror-folded polarization-independent wavelength filter,'' *IEEE Photonics Technol. Lett.* **3**, 219–221 (1991).
30. F. Tian, C. Harizi, H. Hermann, V. Reimann, R. Ricken, V. Rust, W. Sohler, F. Wehrmann, and S. Westenhofer, ''Polarization independent integrated optical, acoustically tunable double-stage wavelength filter in $LiNbO_3$,'' *J. Lightwave Technol.* **12**, 1192–1195 (1994).

Franck Chollet received the electronics engineering degree from the ENSERB, Bordeaux, France, in 1991, and the doctorate degree in Sciences Pour l'Ingénieur from the Université de Franche-Comté, Besançon, France, in 1995 for his work on integrated optics devices for the CNET (France Telecom). He was then with LIMMS, a French-Japanese laboratory, for two years, hosted by H. Fujita at the IIS, University of Tokyo, as a JSPS Post-Doctoral Fellow, where he developed optical MEMS for telecommunication. After working at LPMO, Besançon, France, on micro-cooler and LIGA processes, he became a Research Associate at the IMRE, Singapore, where he developed MEMS optical sensors and switches. Since September 1999 he has been Assistant Professor in the school of Mechanical and Production Engineering at Nanyang Technical University, Singapore, pursuing his work on optical MEMS technology.

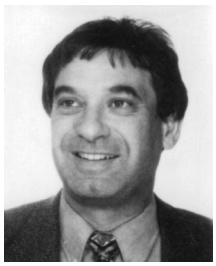

Jean-Pierre Goedgebuer is a professor of physical optics at the University of Franche-Comte, France, and the director of the Laboratorie d'Optique in Besançon. He is also a member of the Institut Universitaire de France. During 1995–2000, he chaired the Electrical and Electronic Engineering Committee at CNRS, Paris. His research includes the areas of optoelectronics and integrated optics, signal processing, optics, and secure communications.

Gadang Ramantoko: Biography and photograph not available.